# Intensity Dependence of Current–Voltage Characteristics and Recombination in High-Efficiency Solution-Processed Small-Molecule Solar Cells

**Aung Ko Ko Kyaw,[†,‡,∥] Dong Hwan Wang,[†,∥] Vinay Gupta,[†,§] Wei Lin Leong,[‡] Lin Ke,[‡] Guillermo C. Bazan,[†] and Alan J. Heeger[†,*]**

[†]Center for Polymers and Organic Solids, University of California at Santa Barbara, Santa Barbara, California 93106-5090, United States, [‡]Institute of Materials Research and Engineering (IMRE), Agency for Science, Technology and Research (A*STAR), Singapore 11760, Republic of Singapore, and [§]Organic and Hybrid Solar Cell Group, CSIR-National Physical Laboratory, Dr. K. S. Krishnan Marg, New Delhi 110012, India. [∥]These authors contributed equally to this work.

**ABSTRACT** Solution-processed small-molecule p-DTS(FBTTh$_2$)$_2$:PC$_{71}$BM bulk heterojunction (BHJ) solar cells with power conversion efficiency of 8.01% are demonstrated. The fill factor (FF) is sensitive to the thickness of a calcium layer between the BHJ layer and the Al cathode; for 20 nm Ca thickness, the FF is 73%, the highest value reported for an organic solar cell. The maximum external quantum efficiency exceeds 80%. After correcting for the total absorption in the cell through normal incidence reflectance measurements, the internal quantum efficiency approaches 100% in the spectral range of 600–650 nm and well over 80% across the entire spectral range from 400 to 700 nm. Analysis of the current–voltage (*J*–*V*) characteristics at various light intensities provides information on the different recombination mechanisms in the BHJ solar cells with different thicknesses of the Ca layer. Our analysis reveals that the *J*–*V* curves are dominated by first-order recombination from the short-circuit condition to the maximum power point and evolve to bimolecular recombination in the range of voltage from the maximum power point to the open-circuit condition in the optimized device with a Ca thickness of 20 nm. In addition, the normalized photocurrent density curves reveal that the charge collection probability remains high; about 90% of charges are collected even at the maximum power point. The dominance of bimolecular recombination only when approaching open circuit, the lack of Shockley–Read–Hall recombination at open circuit, and the high charge collection probability (97.6% at the short circuit and constant over wide range of applied voltage) lead to the high fill factor.

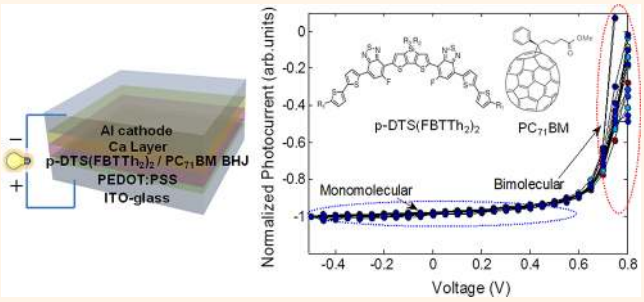


**KEYWORDS:** solution-processed small molecule · bulk heterojunction solar cell · recombination · intensity dependence

Bulk heterojunction (BHJ) organic solar cells based on interpenetrating networks in blends of organic donors and fullerene derivative acceptors have been intensively studied over the past decade for their potential in obtaining clean energy at low costs.[1−3] In these BHJ solar cells, ultrafast photoinduced charge transfer occurs at the interface of phase-separated acceptor and donor and thereby generates mobile holes in the donor phase and mobile electrons in the acceptor phase. These mobile carriers are swept out and transported to the electrodes by the built-in internal electric field. Thus, the carrier collection by sweep-out to the electrodes (driven by the internal field) must take place prior to carrier recombination within the cell.[4] Since recombination results in the loss of photogenerated charge carriers, acquiring an understanding of the mechanisms governing recombination is critical for increasing the short-circuit current density ($J_{sc}$), the fill factor (FF), and for increasing the power conversion efficiency (PCE).

* Address correspondence to ajhe1@physics.ucsb.edu.

Received for review March 12, 2013 and accepted April 18, 2013.

**Published online April 18, 2013**
10.1021/nn401267s

Recombination in conjugated polymer-based BHJ solar cells has been studied by various techniques including transient photoconductivity,[4,5] transient absorption spectroscopy,[6] time-delayed collection field (TDCF) experiment,[7] time-delayed dual pulse experiment,[8] bulk generation time-of-flight,[9] and light-intensity-dependent measurements.[10,11] The loss mechanisms in polymer BHJ solar cells are generally explained in terms of monomolecular and/or bimolecular recombination. Monomolecular recombination historically refers to any first-order process including geminate recombination[5,12] (recombination of a bound geminate electron−hole pair before mobile carriers are created) and Shockley−Read−Hall (SRH) recombination,[13,14] in which an electron and a hole recombine through a trap state or recombination center due to interfacial defects and/or impurities in materials (trap-based recombination). Transient photoconductivity measurements and TDCF experiments carried out on operating solar cells revealed that geminate recombination is not a dominant mechanism in poly (3-hexylthiophene) (P3HT)-based BHJ solar cells.[5,7] For poly[*N*-9″-heptadecanyl-2,7-carbazole-*alt*-5,5-(4′,7′-di-2-thienyl-2′,1′,3′-benzothiadiazole)] (PCDTBT), the geminate recombination is also not significant while SRH recombination at interfacial traps was proposed as the dominant mechanism.[15]

On the other hand, bimolecular recombination refers to the recombination of mobile electrons and holes at the interface of the donor−acceptor heterojunction. In a solar cell with trap-free carriers in the acceptor and donor domains, bimolecular recombination is the dominant recombination mechanism. In bimolecular recombination, mobile carriers recombine to return the system (as a bound pair) to the ground state. This bound pair is metastable, and during its lifetime, it can undergo multiple dissociations with subsequent carrier recombination.[16] According to recent studies, bimolecular recombination depends on the Langevin rate[11,17] and also the distance that free carriers are required to travel in transit to the electrodes.[18]

Recently, solution-processed small-molecule (SM) BHJ solar cells have advanced substantially to efficiencies larger than 7%,[19,20] approaching that of polymer counterparts. Nonetheless, the recombination mechanism in SM BHJ has not been thoroughly explored and is not well-understood. There are only a few studies[21,22] on the recombination losses in SM BHJ. The aim of this work is to understand the recombination mechanisms that determine the charge collection probability ($P_C$) and the effect of applied voltage on the recombination kinetics in SM BHJ solar cells. This is achieved by a straightforward method of accurately measuring the illumination intensity dependence of the current−voltage ($J$−$V$) characteristics.

As demonstrated here, our SM BHJ solar cells based on 7,7′-(4,4-bis(2-ethylhexyl)-4*H*-silolo[3,2-b:4,5-b′]-dithiophene-2,6-diyl)bis(6-fluoro-4-(5′-hexyl-[2,2′-bithiophen]-5-yl)benzo[*c*][1,2,5]thiadiazole) (p-DTS-(FBTTh$_2$)$_2$) donor exhibited PCE = 8.01% and FF ∼ 73% using a 20 nm thick Ca layer capped by aluminum (80 nm). We discovered that increasing the thickness of the Ca layer (up to 20 nm) improves the PCE of the solar cells unprecedentedly. Analysis of the $J$−$V$ characteristics at various light intensities provides information on the different recombination mechanisms in BHJ solar cells with different thicknesses of the Ca layer. Our results show that the kinetics of recombination for the SM BHJ solar cells depend on the external voltage applied to the device; the $J$−$V$ curves are dominated by first-order recombination from the short-circuit condition to the maximum power point and evolve to bimolecular recombination in the range of voltage from the maximum power point to the open-circuit condition in the device with Ca (20 nm thickness), whereas the $J$−$V$ curves are limited by both monomolecular and bimolecular recombination at open circuit in the device with thin Ca (or without any Ca layer). Furthermore, the intensity dependence of $J_{sc}$ and the open-circuit voltage ($V_{oc}$) reveals additional information on recombination in the cells and verifies the results obtained from the light intensity dependence of the $J$−$V$ curves.

In the Results and Discussion, we organized the article as follows: In the first part, we present the characterization of the p-DTS(FBTTh$_2$)$_2$ small molecule (XRD studies of the structure, FET mobility measurements, and AFM images of the surface morphology). The detailed performance of the fabricated p-DTS-(FBTTh$_2$)$_2$:PC$_{71}$BM BHJ devices, including the $J$−$V$ characteristics under AM 1.5G at 100 mW/cm$^2$ and in the dark, and the external and internal quantum efficiencies (EQE and IQE) are presented. The recombination studies are discussed in the second part.

## RESULTS AND DISCUSSION

**Characterization of the SM Donor Material and Performance of Fabricated Devices.** A blend of p-DTS(FBTTh$_2$)$_2$ and [6-6]-phenyl C$_{70}$ butyric acid methyl ester (PC$_{71}$BM) is used as a model system in this study. The molecular structure of p-DTS(FBTTh$_2$)$_2$, PC$_{71}$BM, and the device structure are shown in Figure 1a. We used different thicknesses of Ca (covered by aluminum) in the cathode bilayer (20, 10, and 0 nm) to study the influence of the Ca layer on the recombination of the solar cells. Figure 1b shows the energy levels of individual layers used in the device. The HOMO and LUMO energy levels of p-DTS(FBTTh$_2$)$_2$ are −5.12 and −3.34 eV,[19] and that of PC$_{71}$BM are −6.1 and −4.3 eV, respectively.

The pure p-DTS(FBTTh$_2$)$_2$ exhibits relatively high hole mobility $\mu$ = 0.14 cm$^2$ V$^{-1}$ S$^{-1}$ as obtained from field-effect transistor (FET) measurements in the saturated

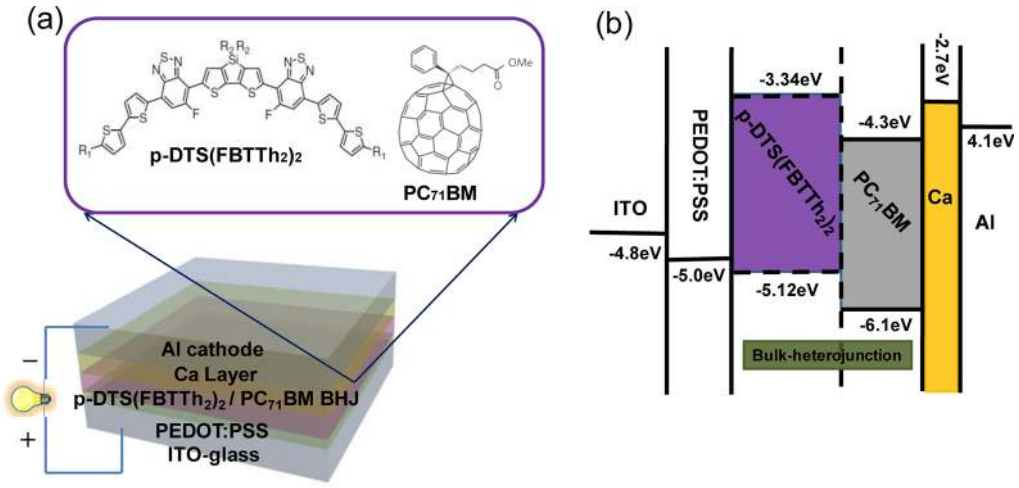


**Figure 1. (a) Molecular structure of p-DTS(FBTTh$_2$)$_2$, acceptor of PC$_{71}$BM, and schematic of the device. (b) Energy level diagram of SM BHJ solar cells with sequential layer of ITO/PEDOT:PSS/p-DTS(FBTTh$_2$)$_2$:PC$_{71}$BM BHJ/Ca layer/Al cathode.**

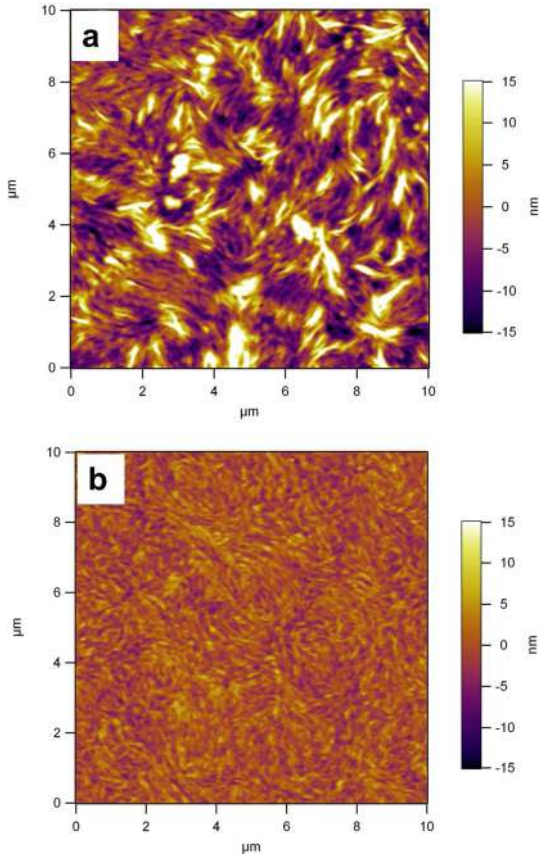


**Figure 2. Atomic force microscopy (AFM) 2D topography image of the (a) pure donor of the p-DTS(FBTTh$_2$)$_2$ and (b) p-DTS(FBTTh$_2$)$_2$/PC$_{71}$BM BHJ film. The scan rate is 1 Hz for all measurements.**

regime (see Supporting Information, Figure S1). The high mobility of p-DTS(FBTTh$_2$)$_2$ can be attributed to the crystallinity which can be seen from the XRD data. AFM images of the pure donor and the p-DTS(FBTTh$_2$)$_2$/PC$_{71}$BM BHJ film are shown in Figure 2. The surface of the film is relatively rough, with variations as large as 3−4 nm in the image obtained from the pure donor. The fibrillar structures persist over distances in excess of 1 $\mu$m in the pure donor film. The fibrillar structures are smaller in the BHJ film yet persist over distances approaching 1 $\mu$m.

The XRD data of the pure donor and the BHJ films are shown in Figure 3a,b. Out-of-plane X-ray scans (Bragg geometry) reveal a sharp peak with high intensity at $2\theta \approx 4°$ ($d \approx 2.2$ nm). The observation of higher order reflections at $2\theta \approx 8$ and 12° indicates that the BHJ film is highly crystalline. Using the Scherrer formula, the coherence length (estimated crystallite size) is ~50 nm for the pure donor. The BHJ film shows higher order reflections even after addition of 40% PC$_{71}$BM is added to form the BHJ layer. The peaks broaden (coherence length of 26.1 nm) and shift slightly to lower $2\theta$ in the BHJ film, indicating that the *d*-spacing increases from 2.2 to 2.3 nm. In-plane incidence X-ray scans reveal fundamental reflection at $2\theta \approx 24.5°$ (the peak at 31.7° arises from the substrate). The *d*-spacing is only 0.336 nm, indicative of $\pi-\pi$ stacking with strong intermolecular interaction along the $\pi-\pi$ stacking direction parallel to the surface of the substrate.

Figure 4 shows the *J*−*V* curves of the SM BHJ solar cells with various thicknesses of Ca layer under illumination of 100 mW/cm$^2$ and in the dark. The PCE critically depends on the thickness of the Ca layer. The PCEs of the SM BHJ solar cells are 5.79, 7.01, and 8.01% for the cells with 0, 10, and 20 nm Ca, respectively. There is also an increase in the FF from 56.1% for the cell without Ca to 72.8% for the cell with 20 nm Ca. However, the FF decreases when the thickness of Ca is more than 20 nm and hence the PCE decreases (see Supporting Information, Figure S2 and Table S1). From the *J*−*V* curves, we observed that a thick Ca (20 nm) layer reduces the series resistance and increases the shunt resistance, leading to improved FF and $J_{sc}$.

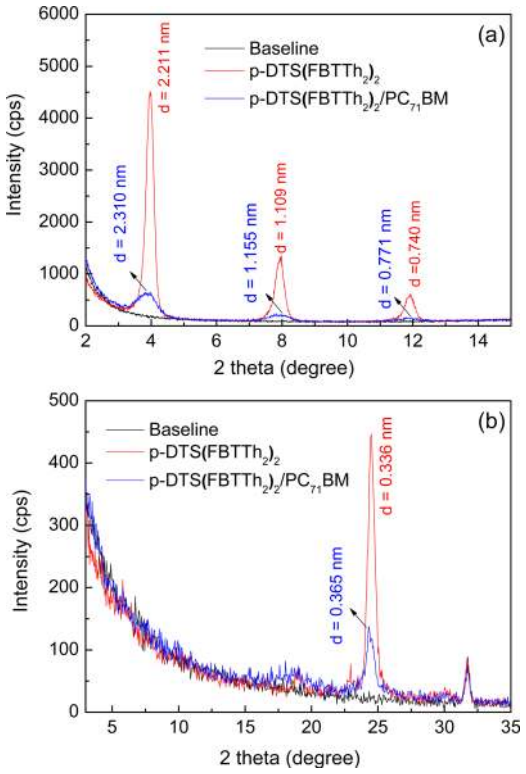


**Figure 3. (a) Out-of-plane X-ray scan with momentum change perpendicular to the surface of the substrate, and (b) in-plane grazing incidence X-ray scan of the pure p-DTS-(FBTTh$_2$)$_2$ and p-DTS(FBTTh$_2$)2:PC$_{71}$BM BHJ film. The crystallinity is confirmed by a Gaussian peak at $2\theta \approx 4$, 8, and 12° ($d \approx 2.2$ nm) for the pure donor and 2.3 nm of BHJ, respectively, at $2\theta \approx 4°$. For the BHJ film, the peak at $2\theta \approx 24°$ indicates $\pi-\pi$ stacking with a $d$-spacing of 0.365 nm.**

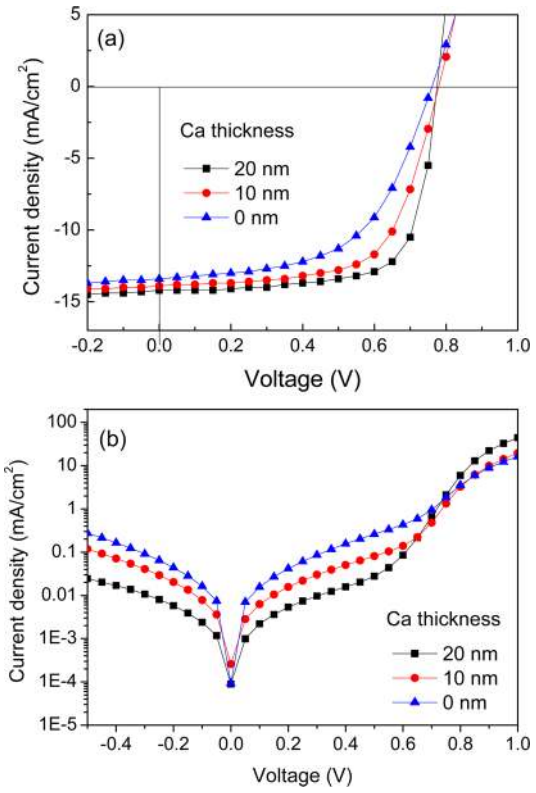


**Figure 4. $J-V$ characteristics of the p-DTS(FBTTh$_2$)$_2$/PC$_{71}$BM BHJ solar cells with 20, 10, and 0 nm Ca (a) under AM 1.5G irradiation at 100 mW/cm$^2$ and (b) in the dark.**

**TABLE 1. Electrical Parameters of the p-DTS(FBTTh$_2$)$_2$:PC$_{71}$BM Solar Cells with 20, 10, and 0 nm Ca**

| Ca thickness | $J_{sc}$ [mA/cm$^2$] | $V_{oc}$ [V] | FF [%] | PCE [%] | $R_s$ [Ωcm$^2$] | $R_{sh}$ [kΩcm$^2$] |
|---|---|---|---|---|---|---|
| 20 nm | 14.2 | 0.775 | 72.8 | 8.01 | 1.8 | 2.0 |
| 10 nm | 13.9 | 0.776 | 64.6 | 7.01 | 6.7 | 0.7 |
| 0 nm | 13.4 | 0.770 | 56.1 | 5.79 | 10.0 | 0.5 |

In addition, the device with a thick Ca layer shows excellent diode quality in the dark $J-V$ curve with very low leakage current and high rectification ratio (forward to reverse factor of approximately 100). The detailed electrical parameters of the cells with various thicknesses of Ca are summarized in Table 1.

Figure 5a shows the EQE spectra of the device without Ca and the device with 20 nm Ca. The EQE value exceeds 80% over the wavelength range of 600 and 700 nm for devices with 20 nm Ca. To fully characterize the performance of the high PCE cells, we also measured the IQE of the p-DTS(FBTTh$_2$)$_2$/PC$_{71}$BM BHJ solar cells, as shown in Figure 5b. The IQE is the ratio of the number of charge carriers collected by the solar cell to the number of photons of given energy that are absorbed by the cell. After correcting the total absorption in the cell through normal incidence reflectance measurements (as illustrated in the inset of Figure 5b),[3,23] the IQE approaches 100% in the spectral range of 600−650 nm and remains well over 80% across the entire spectral range from 400 to 700 nm. The very high IQE values indicate that nearly every absorbed photon is converted to separated charges in the donor and acceptor domains, and that these photogenerated charges are collected at the electrodes.

**Recombination Studies of SM BHJ Solar Cells.** To understand the high performance of p-DTS(FBTTh$_2$)$_2$:PC$_{71}$BM solar cells with the Ca layer, we study the recombination mechanisms in the cells with various thicknesses of Ca using the simple technique of light intensity dependence of $J-V$ characteristics. The $J-V$ characteristics of the p-DTS(FBTTh$_2$)$_2$:PC$_{71}$BM solar cell (20 nm Ca) for the illumination intensities ranging from 100 to 0.9 mW/cm$^2$ are shown in Figure 6a. The total current density ($J_{total}$), which is a function of the light intensity ($I$) and the applied voltage ($V$), can be expressed as a combination of the dark diode current ($J_{dark}$) and the photogenerated current ($J_{ph}$).

$$J_{total}(I, V) = J_{dark}(V) + J_{ph}(I, V) \quad (1)$$

The photocurrent in eq 1 can be written as

$$J_{ph}(I, V) = qLG(I)P_C(I, V) \quad (2)$$

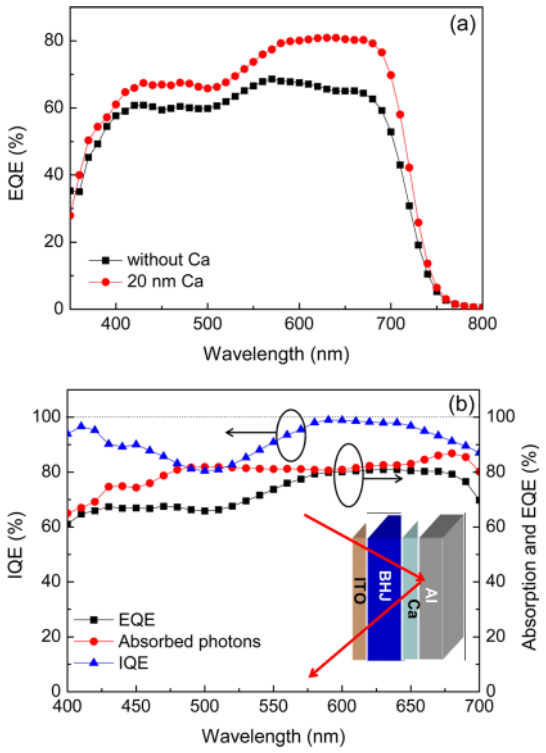


**Figure 5. (a) External quantum efficiency (EQE) spectra of p-DTS(FBTTh$_2$)$_2$/PC$_{71}$BM BHJ solar cells without Ca and with 20 nm Ca. (b) Internal quantum efficiency (IQE) of the solar cell with 20 nm Ca. The inset shows the device structure used in the measurement of total absorption in the cell.**

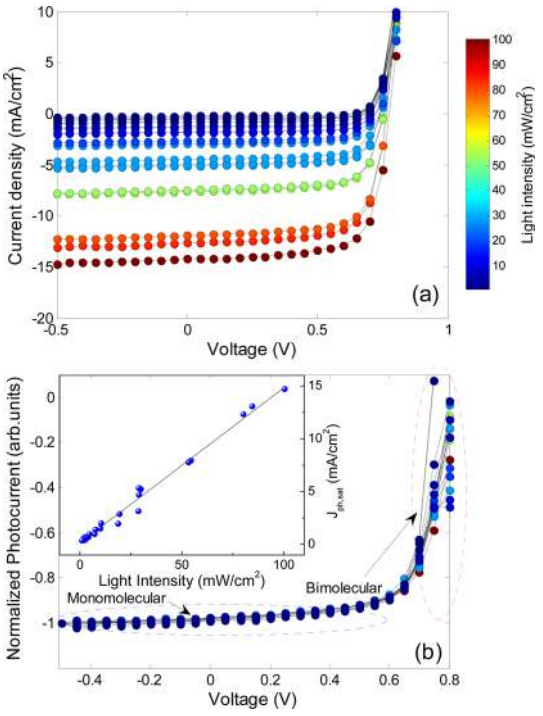


**Figure 6. (a) $J-V$ characteristics of p-DTS(FBTTh$_2$)$_2$:PC$_{71}$BM solar cells with 20 nm Ca under various light intensities ranging from 100 to 0.9 mW/cm$^2$. (b) Charge collection probability (or) photocurrent normalized to reverse saturation photocurrent ($J_{ph,sat}$). The two ovals highlight voltage ranges where monomolecular and bimolecular recombination mechanisms are dominant. Inset: $J_{ph,sat}$ plotted against the light intensity.**

where $q$ is the elementary charge, $L$ is the thickness of the active layer, $G(I)$ is the generation rate of bound electron−hole pairs per unit volume, and $P_C(I,V)$ is the charge collection probability.[4] When it is assumed that the internal field is large enough to sweep out all carriers to electrodes at sufficiently large reverse bias (−0.5 V) and $P_C$ = 1, the reverse saturation photocurrent, $J_{ph,sat}(I) = qLG(I)$. Thus, $P_C(I,V)$ or normalized photocurrent to $J_{ph,sat}$ can be expressed as

$$P_C(I,V) = \frac{J_{ph}(I,V)}{J_{ph,sat}(I)} \quad (3)$$

Herein, it is worth mentioning that $J_{total}$ slightly increases at large reverse bias (−3 V) due to the increase in $J_{dark}$ (higher leakage current with higher reverse bias) but $J_{ph}$ is almost constant over the applied negative voltage (see Supporting Information, Figure S3). Therefore, our assumption that $J_{ph}$ is saturated at −0.5 V is verified.

Figure 6b shows a set of normalized photocurrent data under simulated solar illumination covering an intensity range from 100 to 0.9 mW/cm$^2$. The data are obtained from the measured total current with the dark current subtracted and normalized to $J_{ph,sat}$ using eqs 1 and 3. The $P_C(I,V)$ characteristics are virtually identical at the different light intensities from −0.5 V to approximately 0.65 V, that is, close to the maximum power point (MPP). Moreover, the $J_{ph,sat}$ is linearly proportional to the light intensity (inset of Figure 6b). The intensity independence of the $P_C$ curve over a wide range of illumination intensities and linear variation of $J_{ph,sat}$ with intensity imply that the recombination is dominated by a first-order (monomolecular) mechanism from the short circuit to near the MPP[15,24] with bimolecular contributions playing a secondary role.[7]

In contrast, beyond the MPP where the effective internal field is very low (due to the large applied bias), the $P_C$ curve becomes dependent on the light intensity. The variation in $P_C$ with the intensity is the most prominent at the open-circuit voltage, the externally applied bias at which $J_{total}$ is 0. Generally, bimolecular kinetics would result in an increasing rate of recombination as the intensity increases and a corresponding change in $P_C$.[15] Thus, the dominant mechanism evolves from monomolecular to bimolecular kinetics beyond the MPP, and the recombination mechanism depends on the applied bias (internal electric field). At a given voltage, the competition between sweep-out and recombination determines the carrier density available for recombination within the device. Therefore, the increased carrier density with decreasing internal voltage (decreasing carrier sweep-out) is expected to change the magnitude of bimolecular

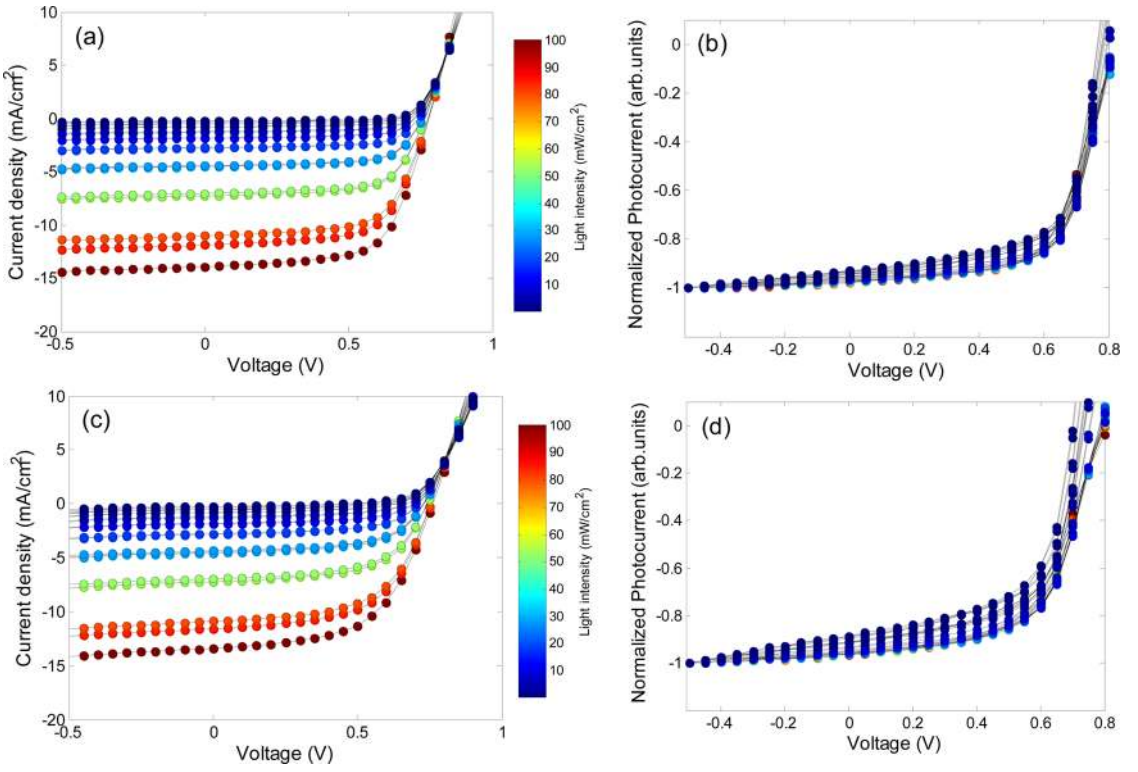


**Figure 7. $J-V$ characteristics (a,c) and the charge collection probability (b,d) of p-DTS(FBTTh$_2$)$_2$:PC$_{71}$BM solar cells with 10 and 0 nm Ca, respectively, under various light intensities ranging from 100 to 0.9 mW/cm$^2$.**

recombination rate and cause the crossover from monomolecular to bimolecular recombination.[10]

We observe that the Ca layer alters the shape of the $P_C$ curve and, in turn, the recombination mechanism in the solar cell. The $J-V$ characteristics of the SM BHJ solar cell without Ca and with a 10 nm Ca layer under various illumination intensities are shown in Figure 7a,c. The normalized photocurrents are shown in Figure 7b,d. In contrast to the cell with Ca thickness of 20 nm, the variation in $P_C$ curves with light intensity is clearly seen at any applied positive voltage in the cell with 10 nm of Ca. A subtle spread in $P_C$ curves is observed even at small negative applied voltage. The spread in $P_C$ curves for various intensities is even more significant in the cell without Ca. Hence, bimolecular recombination is observed at any applied voltage in the cells without a Ca layer and in cells with 10 nm of Ca.

To gain deeper insight into the charge recombination kinetics, we studied the variation of $J_{sc}$ as a function of illumination intensity. Several authors have observed a power law dependence of $J_{sc}$ upon light intensity, using the equation

$$J_{sc} \propto I^{\alpha} \qquad (4)$$

where $\alpha$ is close to unity, which is taken as indicative of weak bimolecular recombination.[24−26] In Figure 8, the data are plotted on a log−log scale and fit to a power law using eq 4. For the device with 20 nm Ca, the fitting of the data yields $\alpha$ = 0.945 (0.984 for upper bound)

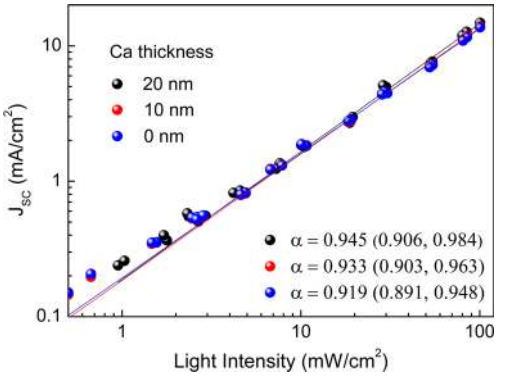


**Figure 8. Measured $J_{sc}$ of p-DTS(FBTTh$_2$)$_2$:PC$_{71}$BM solar cells with 20, 10, and 0 nm Ca plotted against light intensity (symbols) on a logarithmic scale. Fitting a power law (line, eq 4) to these data yields $\alpha$. The values inside the parentheses represent the lower bound and upper bound.**

which is close to unity. The nearly linear dependence of $J_{sc}$ is consistent with sweep-out at short cicuit but also indicates that bimolecular recombination is relatively weak.[24] This is in agreement with the analysis of the $P_C$ curves at various light intensities. Note, however, that $\alpha$ decreases to 0.933 and 0.919 for the device with 10 and 0 nm Ca, respectively.

The deviation from $\alpha$ = 1 is typically attributed to the bimolecular recombination,[11,25] space charge effects, and variations in mobility between the two carriers.[27,28] However, the mobility as determined by field-effect transistor (FET) measurements shows that the electron and hole mobilities in the BHJ film are

$9.5 \times 10^{-3}$ and $7.7 \times 10^{-3}$ $cm^2/V \cdot s$, respectively, implying balanced charge transport (see Figure S4, Supporting Information). We also measured the $J-V$ characteristics of single-carrier devices and then fitted the results using the space-charge-limited current (SCLC) model. The single-carrier diodes reveal the electron and hole mobilities of $2.13 \times 10^{-3}$ and $1.39 \times 10^{-3}$ $cm^2/V \cdot s$, respectively (see Figure S5, Supporting Information). Therefore, space charge effects and variations in mobility between the two carriers are not responsible for the decrease in $\alpha$ for the devices with 10 and 0 nm Ca. Hence, only bimolecular recombination is important.

We note that, because the devices reported here exhibit relatively high efficiency, most of the charge generated at the short circuit, up to 97.6% for the 20 nm Ca device (based on calculated $P_C$), is swept out of the device prior to recombination and collected as current in the external circuit. Note: This high $P_C$ at the short circuit agrees well with the observation that the IQE approaches 100% in the spectral range of 600−650 nm. Thus, from measurements at short circuit, recombination plays a minor role and the differences between devices are only marginally visible. At open circuit, however, there is no current extraction and all of the photogenerated charge carriers recombine. As a result, the recombination mechanisms can be extracted by studying the $V_{oc}$ as a function of generation rate,[4] which can be tuned linearly by variation of the light intensity.

When bimolecular (Langevin) recombination is the sole loss mechanism, the $V_{oc}$ of a BHJ solar cell is given by[10,29]

$$V_{oc} = \frac{E_{gap}}{q} - \frac{kT}{q}\ln\left[\frac{(1 - P_D)\gamma N_C^2}{P_D G}\right] \quad (6)$$

where $E_{gap}$ is the energy difference between the highest occupied molecular orbital (HOMO) of the donor and lowest unoccupied molecular orbital (LUMO) of the acceptor, $q$ is the elementary charge, $k$ is the Boltzmann constant, $T$ is temperature in Kelvin, $P_D$ is the dissociation probability of the electron−hole pairs, $\gamma$ is the Langevin recombination constant, $N_C$ is the effective density of states, and $G$ is the generation rate of bound electron−hole pairs. Since $G$ is the only term directly proportional to the light intensity ($P_D$ and $\gamma$ are independent of it), the slope of the $V_{oc}$ *versus* the natural logarithm of the light intensity gives $kT/q$ for bimolecular recombination.[10,30] When the additional mechanism of SRH recombination is involved, however, SRH competes with bimolecular recombination and the stronger dependence of $V_{oc}$ on light intensity with a slope greater than $kT/q$ is observed.[10,31]

In Figure 9, the slope for the device with 20 nm Ca is $1.07kT/q$, implying that, at open circuit, bimolecular recombination dominates. This supports the earlier

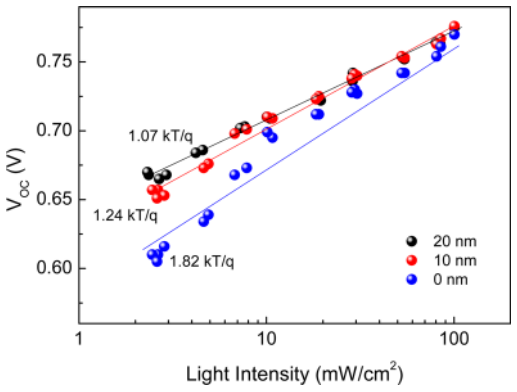


**Figure 9. Measured $V_{oc}$ of p-DTS(FBTTh$_2$)$_2$:PC$_{71}$BM solar cells with 20, 10, and 0 nm Ca as a function of illumination intensity (symbols), together with linear fits to the data (solid lines).**

observation from Figure 6b that monomolecular recombination evolves into bimolecular recombination beyond the MPP. As also shown in Figure 9, the slopes for the device with 10 and 0 nm Ca are $1.24kT/q$ and $1.82kT/q$, respectively. The stronger dependence of $V_{oc}$ on light intensity implies that recombination at open circuit in these devices is a combination of monomolecular (SRH) and bimolecular processes. While the role of Ca in suppressing SRH recombination is not clear, we speculate that Ca might reduce the density of interfacial traps between the acceptor in the BHJ and Al contact. In addition, the lower work function of Ca (2.87 eV), compared to that of Al (4.1 eV), increases the built-in voltage ($V_{bi}$) across the cell. Since the internal voltage ($V_{int}$) is the difference between $V_{bi}$ and the applied voltage in an operating solar cell, larger $V_{bi}$ leads to larger $V_{int}$ at any applied voltage. An increase in $V_{int}$ also might facilitate the charge carriers to escape shallow traps and reduce trap-assisted recombination.

## CONCLUSION

The experiments on intensity-dependent $J-V$ characteristics characterize the recombination mechanisms involved in the p-DTS(FBTTh$_2$)$_2$-based SM BHJ solar cell. For non-optimized devices (10 and 0 nm Ca), bimolecular recombination dominates from short-circuit to open-circuit condition. Monomolecular (SRH) recombination is also observed at open circuit in these devices. In contrast, for an optimized device (20 nm Ca), the recombination evolves from first-order (monomolecular) between the short circuit and MPP to second-order (bimolecular) process beyond MPP. The nearly linear dependence of $J_{sc}$ on light intensity indicates that bimolecular recombination is relatively weak at short circuit, and charge carrier losses in the cell are dominated by monomolecular recombination. The dependence of $V_{oc}$ on the natural logarithm of light intensity with the slope $\sim kT/q$ indicates that bimolecular recombination is the dominant mechanism at

open circuit. In addition, the normalized photocurrent density curves reveal that, in the optimized device, $P_C$ decreases only modestly with increasing applied voltage and about 90% of charges are collected even at the MPP. The dominance of bimolecular recombination only when approaching open circuit, the lack of SRH recombination at open circuit, and the high charge collection probability (97.6% at short circuit and constant over wide range of applied voltage) lead to a high fill factor (~73%).

## METHODS

**Device Fabrication.** The SM BHJ solar cells were prepared by several experimental steps. The ITO was cleaned by detergent, acetone, and isopropyl alcohol with ultrasonication. Then, the ITO was exposed to the UV/ozone treatment to re-form the surface. The hole transport material of PEDOT:PSS (Clevious PH) was spin-coated at 5000 rpm for 40 s to obtain the film thickness of ~30 nm. The p-DTS(FBTTh$_2$)$_2$:PC$_{71}$BM (donor/acceptor) blend solution was prepared from the weight ratio of 60:40 and total 35 mg/mL in CB with 0.4 vol % of DIO processing additive. The solution was dissolved at 60 °C overnight. Before spin-casting, the prepared solution was heated at 90 °C for 15 min. The BHJ film was obtained from spin-casting the solution at 2000 rpm for 45 s. The coated BHJ films were baked to 80 °C for 10 min to evaporate residual solvent. The thickness of the BHJ film is ~100 nm, determined by a surface profiler. Then, the Ca layer was thermally evaporated with the thickness from 0 to 20 nm, and the Al cathode was continuously deposited to ~80 nm at the vacuum condition of $4 \times 10^{-6}$ Torr. The fabricated solar cells were encapsulated with epoxy and cover glass.

FETs with bottom-gate, bottom-contact configuration were fabricated on a heavily n-type-doped silicon wafer with a 200 nm thick $SiO_2$ layer. The n-type-doped Si substrate functioned as the gate electrode, and the $SiO_2$ layer functioned as the gate dielectric. Source and drain electrodes (Au) were deposited by thermal evaporation using a shadow mask. The channel length and width were 20 and 1000 $\mu$m, respectively. The $SiO_2$ surface was passivated with octadecyltrichlorosilane (ODTS). The pristine 20 mg/mL p-DTS(FBTTh$_2$)$_2$ solution in chlorobenzene and the same blend solution used in the fabrication of solar cells were spin-cast at 2000 rpm to form the active layer. After spin-casting, the films were annealed at 80 °C for 10 min on a hot plate. The ODTS treatment and the active layer deposition were carried out in an atmosphere-controlled glovebox filled with $N_2$.

**Device Measurements.** The $J-V$ characteristics of the solar cells were measured by a Keithley 2400 sourcemeter unit. The light source was calibrated by using silicon reference cells with an AM 1.5G solar simulator with an intensity of 100 mW/cm$^2$. During the testing, an aperture with an area of 4.5 mm$^2$ was used to accurately measure the performance of solar cells. In order to test the solar cells under various light intensities, the intensity of the light was modulated with a series of two neutral density filter wheels of six filters apiece, allowing for up to 35 steps in intensity from 100 to 0.4 mW/cm$^2$. The intensity of light transmitted through the filter was independently measured *via* a power meter. All solar cells were tested in ambient air. Characterization of FET was carried out by an analyzer (Keithley 4200 SMU) in the $N_2$-filled glovebox.

**Thin Film Characterization.** The nanomorphologies of pristine p-DTS(FBTTh$_2$)$_2$ film and p-DTS(FBTTh$_2$)$_2$:PC$_{71}$BM BHJ film were investigated by AFM (AFM Asylum MFP3D) to characterize the surface morphology. XRD measurements were carried out by a diffractometer (Rigaku Smartlab high-resolution diffractometer). The films were spin-cast on ITO/PEDOT:PSS and glass for AFM and XRD measurements, respectively. The total absorption by the BHJ layer for IQE calculation was measured by a UV–vis–NIR spectrophotometer system (PerkinElmer Lambda 950) in reflection mode.

*Conflict of Interest:* The authors declare no competing financial interest.

*Acknowledgment.* This research was carried out at UCSB with support from the Department of Energy under a grant titled "Charge Recombination, Transport Dynamics, and Interfacial Effects in Organic Solar Cells"; DOE #DE-FG02-08ER46535. A.K.K.K. thanks Agency for Science Technology and Research (A*STAR) of Singapore for a postdoctoral fellowship. V.G. thanks financial support from Indo-US Science and Technology Forum (IUSSTF), Award No. Indo-US Research Fellowship/2012-2013/26-2012. Authors thank Jason Seifter for XRD measurement and Dr. Sarah Cowan for the Matlab codes used in the data analysis.

*Supporting Information Available:* Transfer and output characteristic of FETs made from pristine p-DTS(FBTTh$_2$)$_2$ film, $J-V$ characteristics of the p-DTS(FBTTh$_2$)$_2$/PC$_{71}$BM BHJ solar cells with 30and 40 nm Ca and their electrical parameters, verification of the saturation of photocurrent at −0.5 V, transfer characteristic of FETs fabricated from p-DTS(FBTTh$_2$)$_2$:PC$_{71}$BM film, and $J-V$ characteristics of the single-carrier devices. This material is available free of charge *via* the Internet at http://pubs.acs.org.

## REFERENCES AND NOTES

1. Yu, G.; Gao, J.; Hummelen, J. C.; Wudl, F.; Heeger, A. J. Polymer Photovoltaic Cells: Enhanced Efficiencies *via* a Network of Internal Donor–Acceptor Heterojunctions. *Science* **1995**, *270*, 1789–1791.
2. Li, G.; Shrotriya, V.; Huang, J.; Yao, Y.; Moriarty, T.; Emery, K.; Yang, Y. High-Efficiency Solution Processable Polymer Photovoltaic Cells by Self-Organization of Polymer Blends. *Nat. Mater.* **2005**, *4*, 864–868.
3. Park, S. H.; Roy, A.; Beaupre, S.; Cho, S.; Coates, N.; Moon, J. S.; Moses, D.; Leclerc, M.; Lee, K.; Heeger, A. J. Bulk Heterojunction Solar Cells with Internal Quantum Efficiency Approaching 100%. *Nat. Photonics* **2009**, *3*, 297–302.
4. Cowan, S. R.; Street, R. A.; Cho, S.; Heeger, A. J. Transient Photoconductivity in Polymer Bulk Heterojunction Solar Cells: Competition between Sweep-Out and Recombination. *Phys. Rev. B* **2011**, *83*, 035205.
5. Street, R. A.; Cowan, S.; Heeger, A. J. Experimental Test for Geminate Recombination Applied to Organic Solar Cells. *Phys. Rev. B* **2010**, *82*, 121301.
6. Marsh, R. A.; Hodgkiss, J. M.; Friend, R. H. Direct Measurement of Electric Field-Assisted Charge Separation in Polymer:Fullerene Photovoltaic Diodes. *Adv. Mater.* **2010**, *22*, 3672–3676.
7. Kniepert, J.; Schubert, M.; Blakesley, J. C.; Neher, D. Photogeneration and Recombination in P3HT/PCBM Solar Cells Probed by Time-Delayed Collection Field Experiments. *J. Phys. Chem. Lett.* **2011**, *2*, 700–705.
8. Mauer, R.; Howard, I. A.; Laquai, F. Effect of External Bias on Nongeminate Recombination in Polythiophene/Methanofullerene Organic Solar Cells. *J. Phys. Chem. Lett.* **2011**, *2*, 1736–1741.
9. Clarke, T. M.; Peet, J.; Nattestad, A.; Drolet, N.; Dennler, G.; Lungenschmied, C.; Leclerc, M.; Mozer, A. J. Charge Carrier Mobility, Bimolecular Recombination and Trapping in Polycarbazole Copolymer:Fullerene (Pcdtbt:Pcbm) Bulk Heterojunction Solar Cells. *Org. Electron.* **2012**, *13*, 2639–2646.
10. Cowan, S. R.; Roy, A.; Heeger, A. J. Recombination in Polymer-Fullerene Bulk Heterojunction Solar Cells. *Phys. Rev. B* **2010**, *82*, 245207.
11. Koster, L. J. A.; Kemerink, M.; Wienk, M. M.; Maturová, K.; Janssen, R. A. J. Quantifying Bimolecular Recombination Losses in Organic Bulk Heterojunction Solar Cells. *Adv. Mater.* **2011**, *23*, 1670–1674.

12. Pal, S. K.; Kesti, T.; Maiti, M.; Zhang, F.; Inganäs, O.; Hellström, S.; Andersson, M. R.; Oswald, F.; Langa, F.; Österman, T.; *et al.* Geminate Charge Recombination in Polymer/Fullerene Bulk Heterojunction Films and Implications for Solar Cell Function. *J. Am. Chem. Soc.* **2010**, *132*, 12440–12451.
13. Shockley, W.; Read, W. T., Jr. Statistics of the Recombinations of Holes and Electrons. *Phys. Rev.* **1952**, *87*, 835–842.
14. Hall, R. N. Electron–Hole Recombination in Germanium. *Phys. Rev.* **1952**, *87*, 387.
15. Street, R. A.; Schoendorf, M.; Roy, A.; Lee, J. H. Interface State Recombination in Organic Solar Cells. *Phys. Rev. B* **2010**, *81*, 205307.
16. Braun, C. L. Electric Field Assisted Dissociation of Charge Transfer States as a Mechanism of Photocarrier Production. *J. Chem. Phys.* **1984**, *80*, 4157–4161.
17. Koster, L. J. A.; Mihailetchi, V. D.; Blom, P. W. M. Bimolecular Recombination in Polymer/Fullerene Bulk Heterojunction Solar Cells. *Appl. Phys. Lett.* **2006**, *88*, 052104.
18. Tumbleston, J. R.; Liu, Y.; Samulski, E. T.; Lopez, R. Interplay between Bimolecular Recombination and Carrier Transport Distances in Bulk Heterojunction Organic Solar Cells. *Adv. Energy Mater.* **2012**, *2*, 477–486.
19. van der Poll, T. S.; Love, J. A.; Nguyen, T.-Q.; Bazan, G. C. Nonbasic High-Performance Molecules for Solution-Processed Organic Solar Cells. *Adv. Mater.* **2012**, *24*, 3646–3649.
20. Kyaw, A. K. K.; Wang, D. H.; Gupta, V.; Zhang, J.; Chand, S.; Bazan, G. C.; Heeger, A. J. Efficient Solution-Processed Small-Molecule Solar Cells with Inverted Structure. *Adv. Mater.* **2013**, 10.1002/adma.201300295.
21. Credgington, D.; Jamieson, F. C.; Walker, B.; Nguyen, T.-Q.; Durrant, J. R. Quantification of Geminate and Nongeminate Recombination Losses within a Solution-Processed Small-Molecule Bulk Heterojunction Solar Cell. *Adv. Mater.* **2012**, *24*, 2135–2141.
22. Proctor, C. M.; Kim, C.; Neher, D.; Nguyen, T.-Q. Nongeminate Recombination and Charge Transport Limitations in Diketopyrrolopyrrole-Based Solution-Processed Small Molecule Solar Cells. *Adv. Funct. Mater.* **2013**, 10.1002/adfm.201202643.
23. Moon, J. S.; Jo, J.; Heeger, A. J. Nanomorphology of PCDTBT:PC70BM Bulk Heterojunction Solar Cells. *Adv. Energy Mater.* **2012**, *2*, 304–308.
24. Riedel, I.; Parisi, J.; Dyakonov, V.; Lutsen, L.; Vanderzande, D.; Hummelen, J. C. Effect of Temperature and Illumination on the Electrical Characteristics of Polymer–Fullerene Bulk-Heterojunction Solar Cells. *Adv. Funct. Mater.* **2004**, *14*, 38–44.
25. Schilinsky, P.; Waldauf, C.; Brabec, C. J. Recombination and Loss Analysis in Polythiophene Based Bulk Heterojunction Photodetectors. *Appl. Phys. Lett.* **2002**, *81*, 3885–3887.
26. van Duren, J. K. J.; Yang, X.; Loos, J.; Bulle-Lieuwma, C. W. T.; Sieval, A. B.; Hummelen, J. C.; Janssen, R. A. J. Relating the Morphology of Poly(*p*-phenylene vinylene)/Methanofullerene Blends to Solar-Cell Performance. *Adv. Funct. Mater.* **2004**, *14*, 425–434.
27. Koster, L. J. A.; Mihailetchi, V. D.; Xie, H.; Blom, P. W. M. Origin of the Light Intensity Dependence of the Short-Circuit Current of Polymer/Fullerene Solar Cells. *Appl. Phys. Lett.* **2005**, *87*, 203502.
28. Mihailetchi, V. D.; Xie, H. X.; de Boer, B.; Koster, L. J. A.; Blom, P. W. M. Charge Transport and Photocurrent Generation in Poly(3-hexylthiophene):Methanofullerene Bulk-Heterojunction Solar Cells. *Adv. Funct. Mater.* **2006**, *16*, 699–708.
29. Koster, L. J. A.; Mihailetchi, V. D.; Ramaker, R.; Blom, P. W. M. Light Intensity Dependence of Open-Circuit Voltage of Polymer:fullerene Solar Cells. *Appl. Phys. Lett.* **2005**, *86*, 123509.
30. Wetzelaer, G. A. H.; Kuik, M.; Lenes, M.; Blom, P. W. M. Origin of the Dark-Current Ideality Factor in Polymer:Fullerene Bulk Heterojunction Solar Cells. *Appl. Phys. Lett.* **2011**, *99*, 153506.
31. Mandoc, M. M.; Veurman, W.; Koster, L. J. A.; de Boer, B.; Blom, P. W. M. Origin of the Reduced Fill Factor and Photocurrent in MDMO-PPV:PCNEPV All-Polymer Solar Cells. *Adv. Funct. Mater.* **2007**, *17*, 2167–2173.